Dynamic and stability analysis of an air pad controlled by a differential diaphragm valve

Dynamic and stability analysis of an air pad controlled by a differential diaphragm valve

Federico Colombo, Luigi Lentini, Terenziano Raparelli, Andrea Trivella

Department of Mechanical and Aerospace Engineering, Politecnico di Torino
Corso Duca degli Abruzzi 24, 10129 Torino

Abstract. The use of pneumatic valves is a simple and economical way to significantly increase the static stiffness of aerostatic pads.
The design procedure of this kind of components consists, firstly, in the optimization of the static performance and, secondly, in a dynamic analysis to assess the stability of the system. This article theoretically analyzes the dynamic behaviour of an aerostatic pad controlled by a custom-built differential diaphragm valve. The stability analysis is performed by means of a lumped parameter model. The equations have been linearized and the bearing stiffness and damping have been investigated using the perturbation method. Subsequently, the paper proposes some functions for verifying the stability of the controlled air pad through Routh-Hurwitz criterion.

Keywords: Compensated air pad, lumped parameter model, Diaphragm valve, Stability.

1 Introduction

Aerostatic pads are widely used in high-precision applications, e.g., machine tools, measuring machines and power board testing [1]. The static and dynamic performance of these devices can be improved by a suitable choice of the size and distribution of the feeding holes [2], [3], [4], [5] or by using porous materials [6]. One possibility to overcome air pad limitations, i.e., low relative stiffness and poor damping, is the use of active and passive compensation methods. Active compensation methods [7], [8], [9], [10] employ control elements of electronic nature which makes them effective even at relatively high frequencies. Passive methods are effective only in static or quasi-static conditions but they are cheaper and simpler with respect to their active counterpart [11] [12]. In passive compensation systems, the regulating action of the supply pressure of the pad can be obtained by modifying the air flow rate provided to the bearing using a nozzle-diaphragm system, located upstream to the bearing [11]. Here, the nozzle-diaphragm distance x_v varies depending on the external load applied upon the pad. The nozzle-diaphragm system is placed inside a pneumatic regulation valve. The diaphragm, whose stiffness is k_v, moves with respect to a nozzle of diameter d_v depending on to the pressure variation in the valve chamber.

The operating point of the regulation, i.e., the initial nozzle-valve distance x_{v0}, can be set using a micrometric screw that modifies the nozzle position. To simplify the set point operation, a second solution for the regulation valve is proposed in [12]. It consists of a valve equipped with three diaphragms and a shutter. Here, the nozzle-shutter distance depends on the pressure difference in two distinct chambers of the valve. The set point is achieved by modifying the reference pressure in one of the two control chambers. It has been experimentally verified that with both the solutions the static stiffness and damping of the controlled bearing are much higher than those of the bearing alone and the control systems are suitable for static or quasi-static loads. With the solutions adopted, no air hammer phenomenon was encountered in the investigated operating conditions. However, it is advisable to analyse the dynamic behaviour in different operating conditions to quantify the likelihood of instability [13], [14]. In [15] the theoretical stability analysis of the system presented in [11] is described; in [16] the dynamic behaviour of the bearing controlled with the solution presented in [12] was studied.
The present work continues the theoretical analysis addressed in [16]: the equations of the numerical model are here linearized both to evaluate the stiffness and damping of the aerostatic pad with the perturbation method, and to study its stability with the Routh-Hurwitz criterion, in different operating conditions.

2 Description of the control system

The controlled air pad is rectangular with dimensions A=110 mm, B=50 mm (Fig. 1). A groove line of dimensions a=80 mm, b=30 mm links four supply holes of diameter d_p= 0.5 mm. The groove has triangular cross-section of dimensions h_g= 60 μm and w_g= 0.3 mm.

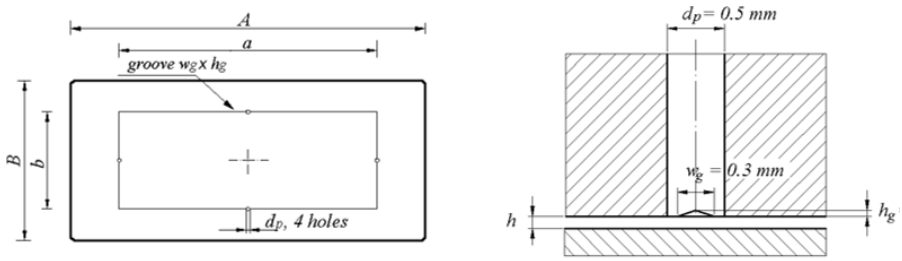

Fig. 1. The geometry of the aerostatic pad.

Fig. 2 shows the functional scheme of the passively compensated system. The nozzle (1), with a diameter d_n = 0.5 mm, is located in the chamber (2) that along with the chamber (3) is supplied with a constant supply pressure P_s. The other chambers (4) and (5) are supplied with $P_{feedback}$ $(= P_f)$ and P_{ref} pressures. The chambers are separated through three flexible diaphragms, two external ones of equal size and a larger central one. The feedback pressure is taken from the air gap under the pad by means of one hole of diameter d_3= 0.25 mm. The supply air flow through the nozzle depends on the distance x_v of the shutter that in turn depends on the difference between P_f and P_{Ref}. The construction section of the differential control valve is described in [10].

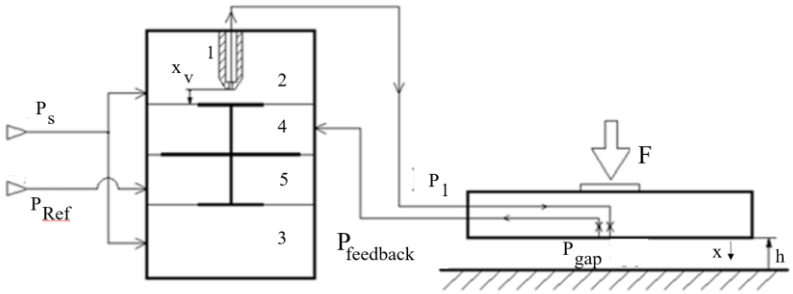

Fig. 2. Functional scheme of the control system.

Once the parameters P_s, P_{Ref}, and the initial distance shutter-nozzle x_{v0} are defined, the valve regulates the air flow depending on the applied vertical load F. The load and the displacement x of the air pad are assumed positive in the shown direction, opposite to the positive direction of h; the speed ẋ is assumed to be positive in the same sense of x.

When the F increases also x increases, then the pressure P_{gap} under the pad and P_f increase too producing a displacement of the shutter and an increase of the air flow that supply the pad. Consequently, the air gap height h increases till a new equilibrium. The opposite holds if F reduces.

3 The numerical model

The equations of the lumped parameter model were described in [12]; they are recalled here to describe the subsequent linearization, that is the subject of the current work. Figure 3 shows the scheme of the model.

R_1, R_2 and R_3 are the resistances of the nozzle, the inlet hole of the air pad and the back pressure hole respectively; R_4 is the resistance of the air gap height. P_2 is the pressure just downstream the resistances R_2, P_{gap} is the mean pressure of the air gap, it is considered uniform in the area surrounded by the groove. V_1 and V_3 are the volumes related to the ducts of the valve and the pad; $V_2 = ABh+V_g$ is the volume under the pad. P_S is the supply pressure and P_a is the ambient pressure. The distance x_v is defined by the equation (1); $x_{by-pass} = 40$ μm is the distance x_v of the minimum air flow rate through the valve. A_v and k_v are the effective area and stiffness of the diaphragms.

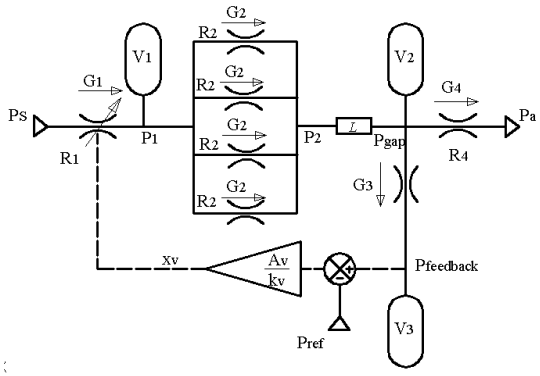

Fig. 3. Pneumatic scheme of the compensated pad.

$$\begin{cases} x_v = x_{by-pass} & x_v \le x_{by-pass} \\ x_v = x_{v0} + A_v \dfrac{(P_f - P_{Ref})}{k_v} & x_v > x_{by-pass} \end{cases} \quad (1)$$

The air mass flow rates passing through R_1, R_2, R_3 (i = 1, 2, 3) are defined by the ISO formula 6358 (2):

$$G_i = K_T\, cd_i\, \psi\, A_i P_{up} \sqrt{1-\varphi_i{}^2}\,;\ \varphi_i = \left(\frac{\frac{P_{down,i}}{P_{up,i}} - b_c}{1-b_c}\right);\ \varphi_i = 0 \text{ if } \frac{P_{down,i}}{P_{up,i}} \le b_c \quad (2)$$

$K_T = \sqrt{T_0/T}$, $T_0 = 293$ K is the reference temperature, T is the absolute temperature. A_i, cd_i, P_{up} and P_{down} are the passage area, the discharge coefficient and the upstream and downstream pressures of the i[th] lumped resistance; b_c=0.528 is the theoretical critical pressure ratio assuming an isentropic expansion; $R = 287.1 \frac{J}{kg\,K}$; $\psi = \frac{0.685}{\sqrt{R\,T}}$; $C_i = cd_i\, \psi\, A_i$ is the conductance of the air passage area. The discharge coefficients are assumed to be functions of the Reynolds' numbers $Re_{c,i}$ and $Re_{a,i}$ related to the flow of each resistance i = 1, 2, 3:

$$cd_i = \begin{cases} 1.05(1 - 0.3\, e^{-0.005\, Re_{a,i}})\ ;\ C_i = \psi\ cd_i\, \pi\, d_i\, x_i\ ;\ \text{if } x_i < \dfrac{d_i}{4} \\ 0.85\ (1 - \ 0.3\, e^{-0.001\, Re_{c,i}}) \left(1 - \ e^{-8.2 \frac{x_i}{d_i}}\right);\ C_i = \psi\ cd_i\ \dfrac{\pi}{4} d_i^2 \quad \text{if } x_i \ge \dfrac{d_i}{4} \end{cases} \quad (3)$$

If i = 1, 3:

$d_1 = d_n$; $x_1 = x_v$; $x_3 = h$; $Re_{c,i} = \frac{4\, G_i}{\pi \mu d_i}$; $Re_{a,i} = \frac{G_i}{\pi \mu d_i}$

If i = 2:

$d_2 = d_p$; $x_2 = h$; $Re_{c,2} = \frac{4\, G_2}{\pi \mu d_2}$; $A_2 = \pi d_2 h + w_g h_g$; $Re_{a,2} = \frac{G_2\, h}{\mu A_2}$

μ is the dynamic air viscosity ($\mu = 18.89 \cdot 10^{-6}$ Pa s). The mass flow rates G_4 exhausted from the air gap under isothermal conditions is shown in (4), P_{gap} is defined by the experimental formula (5), where h is expressed in μm [16, 17]. The load capacity F_p due to the pressure in the air gap is shown in (6). Eq. (7) shows the equilibrium of the forces applied on the pad. M is the mass of the applied load, F includes the weight force of the load.

$$G_4 = \frac{1}{6\mu RT}\left(\frac{b}{A-a} + \frac{a}{B-b}\right)\left(P_{gap}^2 - P_a^2\right) h^3 \quad (4)$$

$$P_{gap} = L\,(h, P_2) = f \cdot (P_2 - P_a) + P_a\ ;\ f = 1 - 0.02^{\left(\frac{5}{h}\right)} \quad (5)$$

$$F_p = \left[ab + AB + \frac{(Ab+aB)}{2}\right]\frac{(P_{gap}-P_a)}{3} \quad (6)$$

$$F - F_P + M\frac{d^2h}{dt^2} = 0 \quad (7)$$

The perturbation method is now applied in order to study the dynamic behavior and the stability of the system. The equations of the mass flow rates are linearized around the static position of the air pad, they are expressed in Laplace domain and shown in (8). The mass flow continuity and the linearization of the equations (1), (5), (6) are shown in (9). The coefficients k_1 ... k_{17} and S_{eq} are analytically defined as the partial derivatives of the equations (1)…(7); they are shown in (10).

$$\begin{aligned}&\overline{G_1} = k_1\overline{x_v} + k_2\overline{P_1};\ \overline{G_2} = k_3\overline{P_1} + k_4\overline{P_2} + k_5\overline{h};\\&\overline{G_3} = k_6\overline{P_{gap}} + k_7\overline{P_f} + k_8\overline{h} = k_9\, s\,\overline{P_f}\\&\overline{G_4} = k_{10}\overline{P_{gap}} + k_{11}\overline{h};\end{aligned} \tag{8}$$

$$\begin{aligned}&\overline{G_1} - 4\overline{G_2} = k_{12}\, s\,\overline{P_1};\ 4\overline{G_2} - \overline{G_3} - \overline{G_4} = k_{13}\, s\,\overline{h} + k_{14}\, s\,\overline{P_{gap}};\\&\overline{P_{gap}} = k_{15}\,\overline{P_2} + k_{16}\,\overline{h};\ \overline{x_v} = k_{17}\,\overline{P_f};\ \overline{F_p} = S_{eq}\overline{P_{gap}};\end{aligned} \tag{9}$$

$$\begin{aligned}&k_1 = \left.\frac{\partial G_1}{\partial x_v}\right|_0;\ k_2 = \left.\frac{\partial G_1}{\partial P_1}\right|_0;\ k_3 = \left.\frac{\partial G_2}{\partial P_1}\right|_0;\ k_4 = \left.\frac{\partial G_2}{\partial P_2}\right|_0;\ k_5 = \left.\frac{\partial G_2}{\partial h}\right|_0;\\&k_6 = \left.\frac{\partial G_3}{\partial P_{gap}}\right|_0;\ k_7 = \left.\frac{\partial G_3}{\partial P_f}\right|_0;\ k_8 = \left.\frac{\partial G_3}{\partial h}\right|_0;\ k_9 = \frac{V_3}{R\,T};\ \ k_{10} = \left.\frac{\partial G_4}{\partial P_{gap}}\right|_0;\\&k_{11} = \left.\frac{\partial G_4}{\partial h}\right|_0;\ k_{12} = \frac{V_1}{R\,T};\ k_{13} = \frac{P_{gap}\,A\,B}{R\,T};\ \ k_{14} = \frac{V_2}{R\,T};\ k_{15} = f;\\&k_{16} = (P_2 - P_a)\left(\frac{5}{h^2}\cdot 0.02^{\frac{5}{h}}\cdot \ln 0.02\right);\\&k_{17} = \frac{A_V}{k_V};\ S_{eq} = \frac{1}{3}\left[ab + AB + \frac{(Ab+aB)}{2}\right]\end{aligned} \tag{10}$$

The solution of the system of equations (8) (9) returns the link between the pressure force F_P and the air gap height h. By defining the following coefficients:

$$\begin{aligned}&a_0 = k_7\,(4k_3 - k_2);\ a_1 = k_9\,(4k_3 - k_2) + k_7\,k_{12};\ a_2 = -k_9k_{12};\\&b_0 = k_1\,k_6\,k_{17} + 4\,k_4\,k_7/k_{15};\ b_1 = -4k_4\,k_9/k_{15};\\&c_0 = k_1\,k_8\,k_{17} - 4k_4\,k_7\,k_{16}/k_{15};\ c_1 = 4\,k_4\,k_9\,k_{16}/k_{15};\ d_0 = -4\,k_3\,k_7;\\&d_1 = 4\,k_3\,k_9;\ e_0 = -k_7\left(\frac{4\,k_4}{k_{15}} - k_{10}\right);\ e_1 = k_9\left(\frac{4\,k_4}{k_{15}} - k_6 - k_{10}\right) + k_7k_{14};\\&e_2 = -k_9\,k_{14};\ f_0 = -k_7\left(4\,k_5 - k_{11} - \frac{4\,k_4k_{16}}{k_{15}}\right);\\&f_1 = k_9\left(4\,k_5 - k_8 - k_{11} - \frac{4\,k_4k_{16}}{k_{15}}\right) + k_7\,k_{13};\ f_2 = -k_9\,k_{13};\\&\tau_1 = \frac{(c_0\,d_1 + c_1\,d_0 - a_0\,f_1 - a_1\,f_0)}{(c_0\,d_0 - a_0\,f_0)};\ \tau_2 = \frac{(c_1\,d_1 - a_1\,f_1 - a_0\,f_2 - a_2\,f_0)}{(c_0\,d_0 - a_0\,f_0)};\ \tau_3 = -\frac{(a_1\,f_2 + a_2\,f_1)}{(c_0\,d_0 - a_0\,f_0)};\\&\tau_4 = -\frac{a_2\,f_2}{(c_0\,d_0 - a_0\,f_0)};\ \gamma_1 = \frac{(a_0\,e_1 + a_1\,e_0 - b_0\,d_1 - b_1\,d_0)}{(a_0\,e_0 - b_0\,d_0)};\ \gamma_2 = \frac{(a_1\,e_1 - b_1\,d_1 + a_0\,e_2 + a_2\,e_0)}{(a_0\,e_0 - b_0\,d_0)};\\&\gamma_3 = \frac{(a_1\,e_2 + a_2\,e_1)}{(a_0\,e_0 - b_0\,d_0)};\ \gamma_4 = \frac{a_2\,e_2}{(a_0\,e_0 - b_0\,d_0)}\end{aligned}$$

We obtain the following transfer function H (11):

$$H(s) = \frac{\overline{F_P}}{\overline{h}} = K_S\,\frac{1+\tau_1 s+\tau_2 s^2+\tau_3 s^3+\tau_4 s^4}{1+\gamma_1 s+\gamma_2 s^2+\gamma_3 s^3+\gamma_4 s^4};\ K_S = S_{eq}\,\frac{(c_0\,d_0 - a_0\,f_0)}{(a_0\,e_0 - b_0\,d_0)} \tag{11}$$

where K_S is the static stiffness of the compensated air pad. Expressing H in the domain of the angular frequency ω we obtain the stiffness K_x and the damping c as functions of the air gap. Equations and coefficients are shown in (12) and (13). K_x is assumed positive when the elastic force on the air pad is opposite to the displacement x, K_x increases as x increases. The damping c is assumed positive when the damping force on the air pad is opposite to the speed $\dot{x}$, c increases as $\dot{x}$ increases.

$$H(\omega) = \mathrm{Re}_H(\omega) + j\,\mathrm{Im}_H(\omega)$$

$$K_x(\omega) = -\,\mathrm{Re}_H(\omega) = -K_S \frac{1 + \alpha_1\omega^2 + \alpha_2\,\omega^4 + \alpha_3\omega^6 + \alpha_4\,\omega^8}{{\lambda_1}^2 + {\lambda_2}^2} \tag{12}$$

$$c(\omega) = \frac{\mathrm{Im}_H(\omega)}{\omega} = K_S \frac{\beta_1 + \beta_2\omega^2 + \beta_3\omega^4 + \beta_4\omega^6}{{\lambda_1}^2 + {\lambda_2}^2}$$

$$\begin{aligned}
&\alpha_1 = (\tau_1\gamma_1 - \tau_2 - \gamma_2);\\
&\alpha_2 = (\tau_2\gamma_2 + \tau_4 + \gamma_4 - \tau_1\gamma_3 - \tau_3\gamma_1);\\
&\alpha_3 = (\tau_3\gamma_3 - \tau_2\gamma_4 - \tau_4\gamma_2);\ \alpha_4 = (\tau_4\gamma_4);\\
&\beta_1 = (\tau_1 - \gamma_1);\ \beta_2 = (\gamma_3 - \tau_3 + \tau_2\gamma_1 - \tau_1\gamma_2);\\
&\beta_3 = (\tau_1\gamma_4 + \tau_3\gamma_2 - \tau_2\gamma_3 - \tau_4\gamma_1);\ \beta_4 = (\tau_4\gamma_3 - \tau_3\gamma_4);\\
&\lambda_1 = (1 - \gamma_2\omega^2 + \gamma_4\omega^4);\ \lambda_2 = \omega(\gamma_1 - \gamma_3\omega^2)
\end{aligned} \tag{13}$$

4 Results and discussion

Figure 4 shows the theoretical trend of the force as a function of the air gap height and the design values chosen for x_{v0} and k_v. The sign reversal of the stiffness of the air gap in the valve adjustment range (overcompensation [7]) is visible. Figure 5 shows the theoretical stiffness and damping trends by imposing a periodic displacement x of frequency f on the pad. ϕ_x is the phase shift between the displacement x and the pressure force F_p in the air gap. The curves for three operating points of the characteristic in Figure 4 are shown, outside and inside the overcompensation zone. The volumes of the connecting ducts were assumed both equal to $V_1 = V_3 = V = 3.4\ cm^3$.

In static conditions the stiffness is much higher than that of the passive bearing but as the frequency increases the stiffness decreases rapidly. It then increases again (and with a positive sign) in a frequency range much higher than that of normal use of the bearing. Even the damping, which is initially very high, rapidly reduces with frequency. For frequencies higher than approximately 10 Hz the phase shift angle ϕ_x becomes negative which indicates a reversal of the sign of the coefficient c. The numerical results confirm that the control system is suitable for static or quasi-static applications.

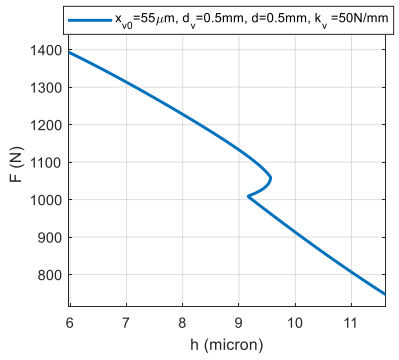

Fig. 4. Static load capacity of the controlled air pad.

To analyze the stability of the air pad is defined: $G(s) = -\frac{1}{Ms^2}$. Therefore the transfer function of the entire system is:

$$\begin{aligned}
G_{eq}(s) &= \frac{\bar{h}}{\bar{F}} = \frac{G(s)}{1 + G(s)H(s)}\\
&= \frac{1}{K_S}\,\frac{(1 + \gamma_1 s + \gamma_2 s^2 + \gamma_3 s^3 + \gamma_4 s^4)}{(1 + \delta_1 s + \delta_2 s^2 + \delta_3 s^3 + \delta_4 s^4 + \delta_5 s^5 + \delta_6 s^6)}
\end{aligned} \tag{14}$$

$$\delta_1 = \tau_1\ ;\ \delta_2 = \tau_2 - \frac{M}{K_S}\ ;\ \delta_3 = \tau_3 - \frac{M\gamma_1}{K_S}\ ;$$

$$\delta_4 = \tau_4 - \frac{M\gamma_2}{K_S};\ \delta_5 = -\frac{M\gamma_3}{K_S};\ \delta_6 = -\frac{M\gamma_4}{K_S}$$

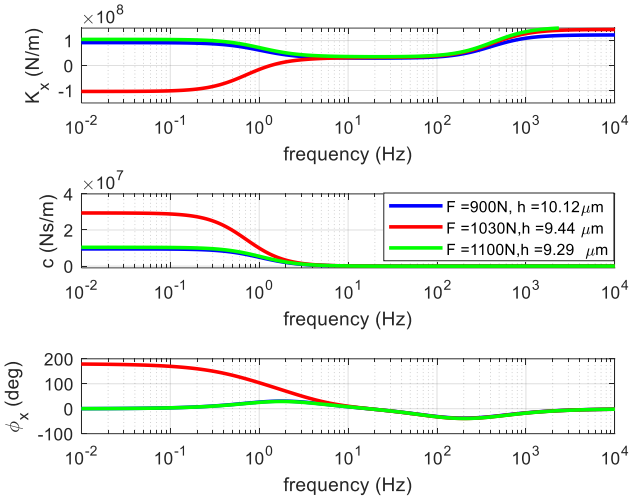

Fig. 5. Dynamic stiffness and damping of the controlled air pad.

The stability of the controlled air pad requires that all the coefficients δ_1, δ_2, δ_3, δ_4, δ_5, δ_6 must be positive and also all the following functions must be positive:

$$\varepsilon_1 = \delta_4 - \frac{\delta_6\,\delta_3}{\delta_5}\ ;\ \varepsilon_2 = \delta_3 - \frac{\delta_2\,\delta_5 - \delta_1\,\delta_6}{\varepsilon_1}\ ;$$
$$\varepsilon_3 = \delta_2 - \frac{\delta_1\,\delta_6}{\delta_5} - \frac{\varepsilon_1\delta_1}{\varepsilon_2} + \frac{\delta_5}{\varepsilon_2}\ ;\ \varepsilon_4 = \delta_1 - \frac{\delta_5}{\varepsilon_1} - \frac{\varepsilon_2}{\varepsilon_3} \qquad (15)$$

We define the stability function S as:

$$S = \eta/\max(|\eta|)\ ;\quad \eta = min(\delta_6, \delta_5, \varepsilon_4, \varepsilon_3, \varepsilon_2, \varepsilon_1) \qquad (16)$$

The system is stable if S > 0. Figure 6 shows the curves of the function S calculated as F varies, assuming three different values of the volume V of the ducts. The other parameters chosen in this simulation (x_{v0}, d_v, d, k_v) are constant and equal to the design parameter shown in Figure 4. To allow the comparison of the results, the η values of each curve were divided by the maximum η value among all three curves. With V equal to the design value (V=3.4 cm^3) the bearing is stable. The most critical zone of the graph is in the valve regulation range, where there is a strong variation of the S values. As V decreases, the respective S values reduce and can become negative, as for curve 3). S < 0 values occur in correspondence of the regulation zone (outside this range S takes on very small positive values).

The reliability of the theoretical stability analysis depend on the correctness of the dynamic model. The results shown in Figure 6 are consistent with the experimental measurements [12] where, under the design conditions, no bearing instability phenomena were detected. To strengthen the validity of the dynamic model created, other experimental tests will be the subject of subsequent work to be conducted in different operating conditions.

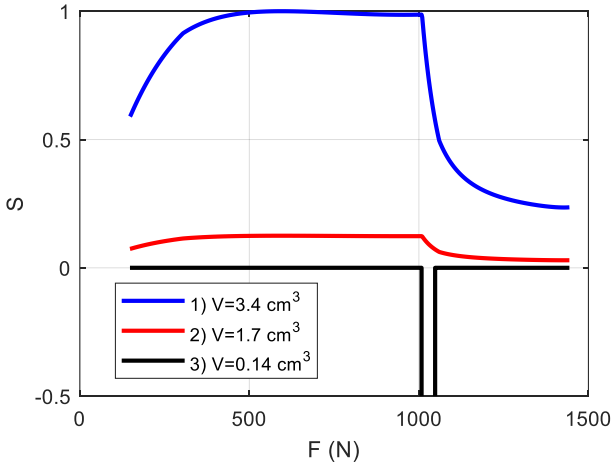

Fig. 6. Stability function S vs. loads F

5 Conclusions

This work describes a theoretical study of the dynamic behaviour of a compensated air pad with a differential pneumatic diaphragm valve. Compared to the single air pad, the passively compensated air pad exhibits significantly higher stiffness and damping for frequencies smaller than about 1 Hertz.

The Routh-Hurwitz criterion was applied to the linearized model of the system, verifying the stability of the air bearing in the design conditions.

The most critical operative condition detected is in the range of F where S declines rapidly, when K_S is negative. An increase of the ducts volume V improves stability.

The Routh-Hurwitz criterion allows immediate verification of the stability of the bearing, avoiding conducting long time-response simulations; the precision of the results depends on the complexity of the adopted dynamic model. The criterion is however valid and more easily applicable to the lumped parameter systems; it can be also used to define parametric maps, useful for quick consultation in design.

Further studies will be aimed to verify the stability of the system by varying other design parameters. The stability margin by applying the Bode or Nyquist criteria will be also analysed.

References

1.Gao, Q., Chen, W., Lu, L., Huo, D., Cheng, K. (2019). Aerostatic bearings design and analysis with the application to precision engineering: State-of-the-art and future perspectives. Trib. Intern. 139, 1-17.

2. Charki, A., Diop, K., Champmartin, S., Ambari, A. (2013). Numerical simulation and experimental study of thrust air bearings with multiple orifices. International Journal of Mechanical Sciences. 72, 28–38.

3 Miyatake, M., and Yoshimoto, S., (2010). Numerical Investigation of Static and Dynamic Characteristics of Aerostatic Thrust Bearings with Small Feed Holes. Tribol. Int., 43 (8), 1353–1359.

4 Li, Y. T., and Ding, H. (2007). Influences of the Geometrical Parameters of Aerostatic Thrust Bearing with Pocketed Orifice - Type Restrictor on Its Performance. Tribol. Int., 40 (7), 1120–1126.

5 Bhat, N., Kumar, S., Tan, W., Narasimhan, R., and Low, T. C. (2012). Performance of Inherently Compensated Flat Pad Aerostatic Bearings Subject to Dynamic Perturbation Forces. Precis. Eng., 36 (3), 399–407.

6 Luong T.S., Potze W., Post J.B., van Ostayen R.A.J., van Beek A. (2004) Numerical and experimental analysis of aerostatic thrust bearings with porous restrictors. Trib. Inter. 37 (10), 825-832.

7. Al-Bender, F. (2009). On the modelling of the dynamic characteristics of aerostatic bearing films: From stability analysis to active compensation. Precis. Eng. 33, 117–126.

8. Maamari, N., Krebs, A., Weikert, S., Wegener, K. (2019). Centrally fed orifice based active aerostatic bearing with quasi-infinite static stiffness and high servo compliance. Trib. Intern. 129, 297–313.

9. Aguirre, G., Al-Bender, F., and Van Brussel, H., (2010). A Multiphysics Model for Optimizing the Design of Active Aerostatic Thrust Bearings. Precis. Eng., 34 (3), 507–515.

10. Colombo, F., Lentini, L., Raparelli, T., Viktorov, V. (2017). Actively compensated aerostatic thrust bearing: design, modelling and experimental validation. Meccanica, 52, 1–16.
11. Ghodsiyeh, D., Colombo, F., Lentini, L., Raparelli, T., Trivella, A., Viktorov, V. (2020). An infinite stiffness aerostatic pad with a diaphragm valve. Trib. Intern. 141, 105964.
12. Colombo, F., Lentini, L., Trivella, A., Raparelli, T. (2024). An aerostatic pad compensated by a differential diaphragm valve. Trib. Intern., 191, 109103.
13. Ma, W., Cui, J., Liu, Y., Tan, J. (2016). Improving the pneumatic hammer stability of aero-static thrust bearing with recess using damping orifices. Trib. Intern. 103, 281–288.
14. Talukder, H. M., and Stowell, T. B. (2003). Pneumatic Hammer in an Externally Pressurized Orifice-Compensated Air Journal Bearing. Tribol. Int., 36 (8), 585–591.
15. Colombo, F., Lentini, L., Raparelli, T., Trivella, A., Viktorov, V. (2021). Dynamic behaviour and stability analysis of a compensated aerostatic pad. 76th Italian National Congress ATI, 15-17 Settembre 2021, Roma, 10.1051/e3sconf/202131205003.
16. Colombo, F., Lentini, L., Raparelli, T., Trivella, A. (2022). Dynamic performance of an aerostatic pad with internal pressure control. 25th AIMETA Conference, Palermo, September 4th-8th, 2022.
17. Colombo, F., Lentini, L., Raparelli, T., Trivella, A., Viktorov, V. (2019). A nonlinear lumped parameter model of an externally pressurized rectangular grooved air pad bearing. Proceedings of the Second International Conference of IFToMM Italy, Cassino, Advances in Italian Mechanism Science, 490-497. Springer International Publishing.